A spectral-domain wave-to-wire model for wave energy converters with a geared rotary electric generator

Tan, Jian; Lavidas, George

DOI
10.36688/ewtec-2025-818

Publication date
2025

Document Version
Final published version

Published in
Proceedings of the European Wave and Tidal Energy Conference

A spectral-domain wave-to-wire model for wave energy converters with a geared rotary electric generator

Jian Tan, George Lavidas

Abstract—**Numerical modelling plays a pivotal role in the design and optimization of wave energy converters. Spectral-domain (SD) modelling has recently received significant research interest as a newly emerging numerical tool. SD modelling is commonly characterized as an extension of frequency-domain (FD) modelling but can incorporate nonlinearities. Thereby, it combines high computational efficiency and adequate accuracy. Previous studies have demonstrated the applicability of SD modelling to a variety of nonlinear hydrostatic/hydrodynamic effects, including viscous drag force, nonlinear hydrostatic force, nonlinear mooring force, etc. However, there also exist influential nonlinear effects in the power generation phase in wave energy conversion. For instance, previous studies have demonstrated that the current limit of the electrical generator could impact the PTO force and the dynamics of the whole system. Therefore, it is necessary to further develop the SD modelling to cover the entire wave-to-wire process in WECs.**

In this paper, an SD model is derived to simulate the wave-to-wire process of a point absorber WEC. A mechanical PTO system coupled with a rotary permanent-magnet generator is considered for the WEC. Representative nonlinear effects of the wave-to-wire process are incorporated, including viscous drag force, nonlinear PTO force, and the current limit of the generator. A nonlinear time-domain (TD) wave-to-wire model is established correspondingly to serve as the accuracy reference because it is inherently associated with higher modelling fidelity. The dynamic response and the power performance of the proposed SD model are verified against those of the nonlinear TD wave-to-wire model. Additionally, the computational efficiency of the proposed SD model and the TD model is identified and compared.

Index Terms—**Wave energy converter, spectral domain modeling, wave-to-wire modeling, geared electric generator**

I. Introduction

As a clean energy resource, ocean waves hold immense potential for renewable energy conversion. However, wave energy converter (WEC) technology has yet to reach large-scale commercialization. Enhancing the competitiveness of existing WECs requires continuous refinement of their design and technology. Due to their efficiency and cost-effectiveness, numerical models play a crucial role in this process, accelerating WEC development.

Wave-to-wire (W2W) modeling is a numerical approach used to assess WEC performance [1]. It provides a comprehensive analysis of the entire energy conversion process, from wave interactions to electricity generation [2]. By integrating multiple stages of energy transformation, W2W models offer deeper insights than purely hydrodynamic models. Over the years, several W2W models have been developed and validated [3]–[5].

While hydrodynamic models typically optimize Power Take-Off (PTO) parameters to maximize the absorbed mechanical power [6], [7], recent studies have shown that this approach does not necessarily lead to high electrical output, as the efficiency of the electrical generator also varies significantly with operating conditions [8], [9]. Hence, optimizing mechanical power absorption does not necessarily equate to optimal electrical power generation. Moreover, generator efficiency fluctuates with WEC operating conditions [10], [11]. For instance, a linear generator in a point absorber may achieve 70% efficiency in high-frequency waves but only 20% in low-frequency conditions. Neglecting generator dynamics can lead to inaccurate PTO parameter estimates. Therefore, incorporating electrical generator modeling into W2W frameworks is essential for more accurate WEC optimization.

Most existing W2W models operate in the time-domain (TD) to account for nonlinear effects in power absorption, transmission, and conversion. However, since WEC technology is still evolving, design optimization demands extensive computational resources. Thus, developing more efficient W2W models is critical to advancing WEC technology towards commercialization.

Spectral-Domain (SD) modeling has gained attention as a computationally efficient alternative. Studies show it can be thousands of times faster than TD modeling while maintaining an error margin below 5% in operational conditions [12], [13]. Unlike conventional Frequency-Domain (FD) approaches, SD modeling incorporates nonlinear effects through statistical linearization, assuming a Gaussian system response [14]. One of its earliest applications involved a flap-

This research was funded by the Dutch Research Council (Nederlandse Organisatie voor Wetenschappelijk Onderzoek-NWO) (EP.1602.22.001) and the CETPartnership, the Clean Energy Transition Partnership under the 2022 CETPartnership joint call for research proposals, co-funded by the European Commission (GAN°101069750) Project No CETP-2022-00127.

Jian Tan (j.tan-2@tudelft.nl) and George Lavidas (G.Lavidas@tudelft.nl) are affiliated are with Faculty of Civil Engineering and Geosciences (CEG), Delft University of Technology, Netherlands.

Digital Object Identifier:
https://doi.org/10.36688/ewtec-2025-818

type WEC with quadratic damping and wave force decoupling, demonstrating strong agreement with TD results [12]. Since then, SD modeling has been extended to account for nonlinear forces such as end-stop, mooring, viscous drag, Coulomb damping, and PTO constraints [13], [15]–[19].

Although SD modeling has proven effective for evaluating the hydrodynamics of WECs, there is a lack of work addressing the development of SD modeling to describe W2W process of WECs. Only recent studies [20], [21] developed a W2W model entirely represented in the spectral domain and verified against higher-fidelity TD models. However, the PTO system of the developed SD W2W model was limited to a linear generator, which severely hinders its applications to different types of WEC designs. Given the variability of PTO systems applied in WECs, W2W models are expected to possess wide applicability. In this sense, further research is needed to bridge this gap.

This work aims to develop an SD model to systematically evaluate the W2W process of a heaving point absorber with a geared rotary PM generator. The proposed model could reveal the statistical properties of various performance indicators of the WEC system, such as dynamic motions, mechanical losses, electrical losses, and produced electrical power. Multiple significant nonlinear effects are incorporated in the model, including PTO force saturation, viscous drag force, friction losses and the current limit. This work presents, to the best of our knowledge, the first SD W2W model to incorporate a rotary PM generator with realistic nonlinearities. As such, it constitutes the first SD W2W model of this particular class of PTO systems which are adopted in WEC prototypes, such as Corpwer. A corresponding nonlinear TD W2W model is utilized as the verification reference, and a variety of operation conditions are taken into account in the verification.

II. WEC SYSTEM DESCRIPTION

The studied WEC concept is illustrated in Figure 1. The WEC system contains two main components: the floating captor and the PTO system. The floating captor is represented by a spherical buoy with a diameter of 5 m. Designed to partially submerge in calm water, the buoy has a density half that of water. Incoming waves trigger vertical oscillations, converting wave energy into mechanical power. Comparatively, the PTO system converts the mechanical motion of the floater to usable electrical power. The floating buoy is connected to the PTO system by a rod. The PTO system consists of a rack-pinion system, a rotary PM generator and a back-to-back voltage converter. The linear movement of the floating buoy is converted to circular motion by the rack and pinion system, which is then used to drive the rotary PM generator. The electrical inverter, connected to the output side of the machine, is implemented as a three-phase back-to-back converter [22]. The design of this generator is inspired by the electrical machine used in the work [23] for a generator concept for wind turbines. However, it has been scaled down from the original reference machine to match the dimensions of the buoy employed in this study. The scaling process follows the principle of maintaining an identical force density per unit area of the active surface of the electrical machines. More detailed information regarding the scaling of electrical machines can be found in [11]. The machine parameters considered in this study are outlined in Table I.

III. METHODOLOGY

This section first outlines the conventional approach for deriving the W2W model in the TD context. Then, it presents the mathematical representation of SD modeling and introduces statistical linearization to incorporate relevant nonlinear effects.

A. Time-domain approach

1) Representation of incoming waves: Incident waves are modeled using linear wave theory [24]. Based on superposition, irregular waves are expressed as

$$\eta_{irr}(t) = \sum_{j=1}^{N} \zeta_a(\omega_j) \cos\left(k(\omega_j)x - \omega_j t + \varphi(\omega_j)\right) \quad (1)$$

where η_{irr} is the wave elevation of irregular waves,t is time, and $k(\omega_j)$, $\zeta_a(\omega_j)$, and $\varphi(\omega_j)$ represent the wave number, amplitude, and phase of the regular wave component at frequency ω_j. Although this work applies the JONSWAP spectrum, expression (1) remains valid for various wave spectra [25]. For a predefined wave spectrum, the amplitude of the wave component is related to the wave energy spectrum S_{ζ_a}, as

$$\zeta_a(\omega_j) = \sqrt{2S_{\zeta_a}(\omega_j)\Delta\omega} \quad (2)$$

2) Hydrodynamic modeling: The floating buoy's interaction with incoming waves is characterized via hydrodynamic modeling, with motion restricted to heave. The buoy's dynamics in the TD framework follow the Cummins equation [26]:

$$\left[M + M_r(\infty)\right]a(t) = F_e(t) + F_{rack}(t) + F_{hs}(t) + F_{vis}(t) + \int_{-\infty}^{t} K_{rad}(t-\tau)u(\tau)d\tau \quad (3)$$

where:

- M is the buoy mass,
- F_e the excitation force,
- F_{hs} the hydrostatic force,
- K_{rad} the radiation impulse function,
- F_{rack} the reaction force on the rack (related to the generator force F_{ge}),
- u and a the buoy velocity and acceleration,
- F_{vis} the viscous drag force.

The terms $M_r(\infty)$ and K_{rad} represent added mass at the limit of infinite frequency and the radiation impulse response function, respectively, derived from hydrodynamic damping $R_r(\omega)$ and added mass $M_r(\omega)$. These hydrodynamic coefficients are derived using the Boundary Element Method (BEM) tool Nemoh [27].

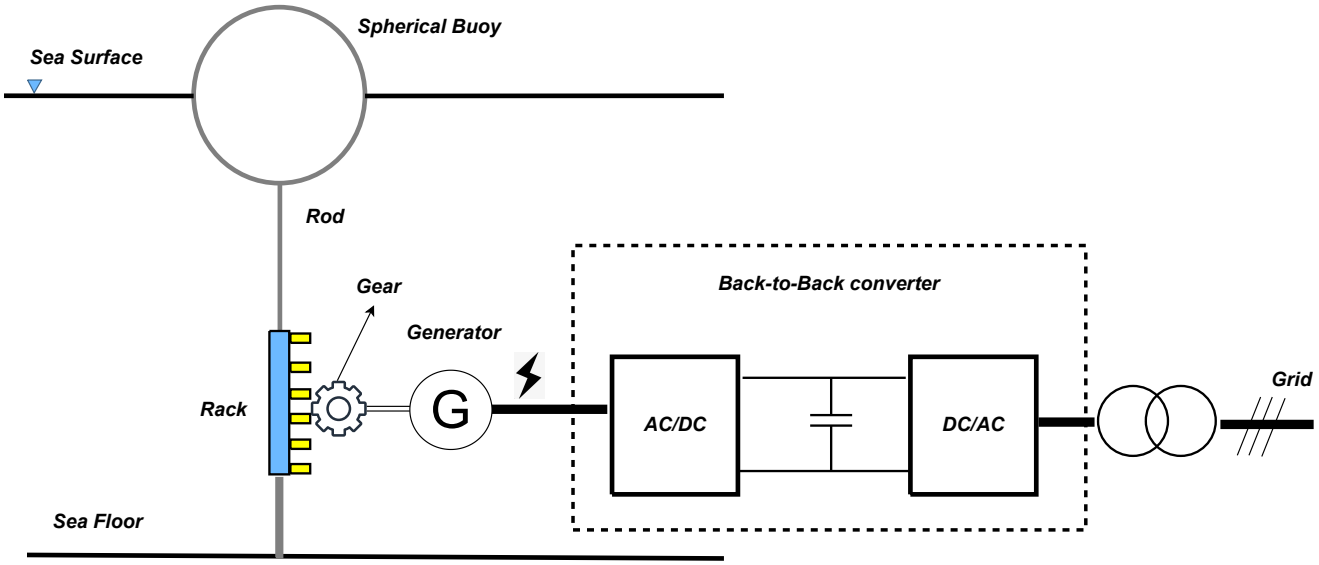

Fig. 1: Schematic of the spherical heaving point absorber with a bottom-founded geared rotary PM generator [10].

TABLE I: Specification of the sized generator.

Parameters	Symbol	Quantities
Maximum average power	$\mathrm{P}_{\mathrm{rated}}$	157 kW
Maximum torque	τ_{ge}	20 kNm
Rated rotation speed	$-$	75 rpm
Rotor radius	r_r	0.41 m
Rotor yoke height	h_{ry}	40 mm
Rotor pole width	b_{rp}	82 mm
Stack length	l_s	0.4 m
Air gap length	g	3.6 mm
Stator slot width	b_{ss}	15 m
Stator yoke height	h_{sy}	40 mm
Stator slot height	h_{ss}	80 mm
Magnet pole width	b_p	79 mm
Magnet pole pairs	p	13
Magnet thickness	l_m	15 mm
Recoil permeability of the magnets	μ_{rm}	1.1
Remanent flux density of the magnets	B_{rm}	1.1 T at 85 °C
Iron loss per unit mass	P_{Fe0}	4.9 W/kg at 50 Hz and 1.5 T
Copper resistivity	ρ_{Cu}	0.0252 $\mu\Omega$m at 120 °C
Copper fill factor	k_{sfil}	0.6
Number of conductors per slot	N_s	6
Number of slots per pole per phase	N_p	1

To enhance computational efficiency, the convolution integral of the radiation force is approximated using a state-space representation [28].

Following [17], the viscous drag force is approximated as a quadratic damping force:

$$F_{vis} = -\frac{1}{2}\rho C_D A_D |u(t)|u(t) \tag{4}$$

where ρ is water density, C_D the drag coefficient, and A_D the buoy's characteristic area perpendicular to motion. The drag coefficient values are based on [29], which studied a geometry identical to the present work.

The maximum torque that the rotary generator could produce imposes a force limit on the rack. In other words, the rack force from the PTO system to the buoy will be saturated once it goes beyond the limit. In this sense, the rack force F_{rack} is given as:

$$F_{rack}(t) = \begin{cases} -R_{rack}u(t), \ \textit{if} \ \ |R_{pto}u(t)| \leq F_{rack_{\mathrm{m}}} \\ \\ \mathrm{sign}[-u(t)]F_{rack_{\mathrm{m}}}, \ \textit{if} \ \ |R_{rack}u(t)| > F_{rack_m} \end{cases} \tag{5}$$

where F_{rack_m} denotes the maximum force limit that the generator could provide via the rack and pinion system to the floater.

3) Rack and pinion modeling: The rack-pinion mechanism converts the linear motion of the floater to circular motion, driving the rotary generator. The kinematic relation between the rack and pinion is expressed as

$$\omega_p = R_{rp}u_r \tag{6}$$

where ω_p is the angular velocity of the pinion, R_{rp} is the rack-pinion gear ratio, and u_r is the velocity of the rack.

The shaft torque of the pinion τ_p can be related to the force on the rack as

$$F_{rack} = -R_{rp}\tau_p \tag{7}$$

As the pinion is directly connected to the generator, the generator torque is equal to the pinion torque, expressed as

$$\tau_p = \tau_{ge} \tag{8}$$

Similarly, there exists the relation:

$$\omega_p = \omega_{ge} \tag{9}$$

where ω_{ge} is the speed of the rotor of the rotary generator.

Substituting (8) into (7) gives

$$F_{rack} = -R_{rp}\tau_{ge} \tag{10}$$

Substituting (9) into (6) gives

$$\omega_{ge} = R_{rp}u_r \tag{11}$$

4) Generator modeling: In this study, an analytical electrical model is utilized to evaluate the performance of the linear generator. The primary function of the linear generator is to convert the absorbed mechanical energy into usable electricity. The design parameters of the generator can be found in Table I. According to [22], the responses of the generator to the motion of the buoy can be described using an analytical model. As the buoy's movement causes relative motion between the translator and stator of the machine, it induces a no-load voltage, which can be calculated as follows:

$$E_p(t) = \sqrt{2}\omega_{ge}(t)pr_l s N_s k_w |\hat{B}_{gm}| \tag{12}$$

where $\hat{B}_{gm}$ is the fundamental space harmonic of the magnetic flux density in the air gap resulting from the magnets [22], p is the number of pole pairs, r_r is the radius of the rotor, l_s is the stack length, N_s is the number of conductors per slot, and k_w is the winding factor.

The iron losses are dependent on the generator frequency, which can be calculated as

$$P_{Fes} = P_{Fe0}\big[M_{Fest}\big(\frac{\hat{B}_{st}}{B_0}\big)^2 + M_{Fesy}\big(\frac{\hat{B}_{sy}}{B_0}\big)^2\big]\frac{f_e}{f_0} \tag{13}$$

where P_{Fe0} is the iron loss per unit mass at the frequency f_0 and flux density B_0; M_{Fest} and M_{Fesy} are the mass of the stator teeth and the stator yoke respectively; f_e is the electrical generator frequency which is dependent on the mechanical angular speed of the rotor, and $\hat{B}_{st}$ and $\hat{B}_{sy}$ embody the fundamental space harmonic of magnetic flux density in the stator teeth and yoke. $\hat{B}_{st}$ and $\hat{B}_{sy}$ can be calculated as

$$\hat{B}_{st} = \hat{B}_{gm}\frac{\tau_s}{b_t} \tag{14}$$

$$\hat{B}_{sy} = \hat{B}_{gm}\frac{\tau_p}{\pi h_{sy}} \tag{15}$$

where τ_s and τ_p are the slot pitch and pole pitch; b_t and h_{sy} are the tooth width and stator yoke height. The generator frequency is calculated as

$$f_e(t) = \frac{\pi|u(t)|}{\tau_p} \tag{16}$$

The power taken by the generator winding is expressed as the balance of absorbed mechanical power from iron losses, and it is expressed as

$$P_{wd} = \tau_{ge}(t)\omega_{ge}(t) - P_{Fes} - P_{fri} \tag{17}$$

where P_{fri} is the friction losses due to mechanical wear. During operation, the iron and friction losses are negligible compared with the absorbed power [10]. Besides, in order to achieve higher system efficiency, the stator current I_s is mostly regulated to be in phase with the no-load voltage E_p [22]. Therefore, (17) can be updated as

$$P_{wd} \approx \tau_{ge}(t)\omega_{ge}(t) = mE_p(t)I_s(t) \tag{18}$$

where m represents the phase number of the electrical machine, and it is three in this case. It can be deduced from (18) that the linkage between the generator modeling and hydrodynamic modeling is built based on the balance between the power taken by the winding and the absorbed mechanical power. Substituting (12) to (18) gives the expression of the stator current:

$$I_s(t) = \frac{\tau_{ge}(t)}{m\sqrt{2}pr_l s N_s k_w |\hat{B}_{gm}|} \tag{19}$$

In electrical machines, there is an additional nonlinearity introduced by the electronic components, specifically the stator current limit I_{limit}. When the stator current approaches the limit, it reaches a saturation point and cannot increase further. The stator current limit is typically implemented to prevent the generator from overheating. It plays a significant role in determining the delivered grid power and overall system performance. Therefore, accounting for this effect is crucial in accurately evaluating the system's performance and ensuring its proper operation. As observed from equation (19), the stator current is directly linked to the PTO force. Consequently, the saturation of the PTO force is intrinsically influenced by the current limit. The impact of the current limit is equivalent to that of the PTO force limit in hydrodynamic modeling. Hence, there is no need to separately incorporate the stator current constraint in the generator modeling. For a given electrical machine, the force limit τ_{ge_m} is correlated with the stator current limit I_{limit} in the following manner:

$$\tau_{ge_m} = m\sqrt{2}pr_l s N_s k_w |\hat{B}_{gm}| I_{limit} \tag{20}$$

After the current I_s is derived, the copper losses can be calculated as

$$P_{copper}(t) = mI_s^2(t)R_t \tag{21}$$

where R_t is the stator phase resistance. For simplification, the converter losses P_{conv} are assumed to be only

related to the generator side in this model, which can be expressed as

$$P_{conv} = \frac{P_{convm}}{31}\left[1 + 20\frac{|I_s(t)|}{I_{sm}} + 10\left(\frac{I_s(t)}{I_{sm}}\right)^2\right] \tag{22}$$

where P_{convm} is the power dissipation in the converter at the rated operating point, and it is assumed to be 3 % of the converter's rated power [30]; I_{sm} is rated current of the converter. In (22), the first term is a small constant part standing for the power dissipated in power supplies, gate drivers, control, and cooling system; the second term accounts for the major part that is proportional to the current, and this part is mainly related to the switching losses and conduction losses; the third term is proportional to the current squared, which corresponds to the conduction losses [30].

The friction losses of the rack and pinion system are assumed to be proportional to rotor speed, and it can be expressed as

$$P_{gear}(t) = P_{gearm}\frac{|\omega_{ge}(t)|}{\omega_{rated}} \tag{23}$$

where ω_{rated} is the rated speed of the generator, P_{gearm} is the friction losses of the rack and pinion system at the rated speed of the rotor, and it is assumed to be 1 % of the rated power of the generator, referring to [23].

As the electrical losses have been derived, the electrical power delivered to the grid can be expressed as

$$P_{grid}(t) = P_{wd}(t) - P_{copper}(t) - P_{Fes}(t) - P_{gear}(t) - P_{conv}(t) \tag{24}$$

B. Spectral-domain approach

SD models are developed within the framework of FD modeling. In SD modeling, nonlinear effects are represented by equivalent linear coefficients in the equations of motion. These equivalent linear coefficients are determined through the process of statistical linearization. Previous studies in the literature have primarily focused on using SD models to predict the hydrodynamic responses of WECs [12], [15], [17], [31]. However, in this subsection, the SD modeling approach is extended to encompass the responses of electrical machines as well. The typical nonlinear effects arising from the electrical generator are linearized and incorporated into the SD model. By integrating these developments, the derived model allows for the calculation of the entire wave-to-wire responses using a purely SD approach. Figure 2 provides a visual representation of the structure and solution process of the proposed SD W2W model.

1) Hydrodynamic modeling: According to Newton's second law, the motion of the WEC as a rigid body in FD can be described as

$$\hat{F}_e(\omega) = [R_r(\omega) + R_{rack,eq} + R_{vis,eq}]\hat{u}(\omega) + \mathrm{i}\omega\hat{u}(\omega)[M + M_r(\omega)] + \mathrm{i}\hat{u}(\omega)(-\frac{K_{hs}}{\omega}) \tag{25}$$

where $R_r(\omega)$ is the hydrodynamic damping coefficient, R_{rack} is the PTO damping coefficient, ω is the angular wave frequency, $M_r(\omega)$ is the added mass of the buoy, $\hat{u}$ is complex amplitude of the vertical velocity, K_{hs} is the hydrostatic stiffness, and $R_{rack,eq}$ and $R_{vis,eq}$ represent the equivalent linear coefficients for the PTO force saturation and viscous force. Then, by solving (25), the complex amplitude of velocity $\hat{u}$ could be obtained as

$$\hat{u}(\omega) = \frac{\hat{F}_e(\omega)}{R_r(\omega) + R_{rack,eq} + R_{vis,eq} + \mathrm{i}\omega[M + M_r(\omega)] - \mathrm{i}\frac{K_{hs}}{\omega}} \tag{26}$$

In a predefined wave spectrum, the amplitude of the wave component is related to the wave energy spectrum S_{ζ_a} [32], as

$$\zeta_a(\omega_j) = \sqrt{2S_{\zeta_a}(\omega_j)\Delta\omega} \tag{27}$$

The variance of the wave elevation $\sigma^2_{\zeta a}$ is calculated as

$$\sigma^2_{\zeta a} = \sum_{j=1}^{N} S_{\zeta_a}(\omega_j)\Delta\omega \tag{28}$$

where $\sigma_{\zeta a}$ is the standard deviation of the wave elevation. Similarly, as the velocity amplitude of WEC corresponding to each wave component can be obtained by (26), the standard deviation and spectral density of the WEC response can be calculated. Then, the mean absorbed power can be derived as

$$\begin{aligned}\overline{P}_{ab} &= \sum_{j=1}^{N}\frac{1}{2}R_{rack,eq}\,|\hat{u}(\omega_j)|^2 \\ &= \sum_{j=1}^{N} R_{rack,eq}S_u(\omega_j)\Delta\omega \\ &= R_{rack,eq}\sigma_u^2\end{aligned} \tag{29}$$

where S_u and σ_u denote the spectral density and standard deviation of the velocity of the WEC.

2) Generator modeling: While the hydrodynamic model described earlier is capable of predicting the mechanical power absorbed by the buoy, it does not capture the conversion of absorbed power into delivered electrical power, which is influenced by the electrical responses of the system. However, by assuming random phase distribution of wave inputs to the WEC system, it is feasible to represent the generator responses within the framework of SD modeling. This allows for the inclusion of electrical aspects and facilitates the description of the generator's behavior in the SD context.

Based on (12), the complex amplitude of the no-load voltage in each frequency component is expressed as

$$\hat{E}_p(\omega) = \sqrt{2}\hat{u}(\omega)pr_r l_s N_s k_w|\hat{B}_{gm}| \tag{30}$$

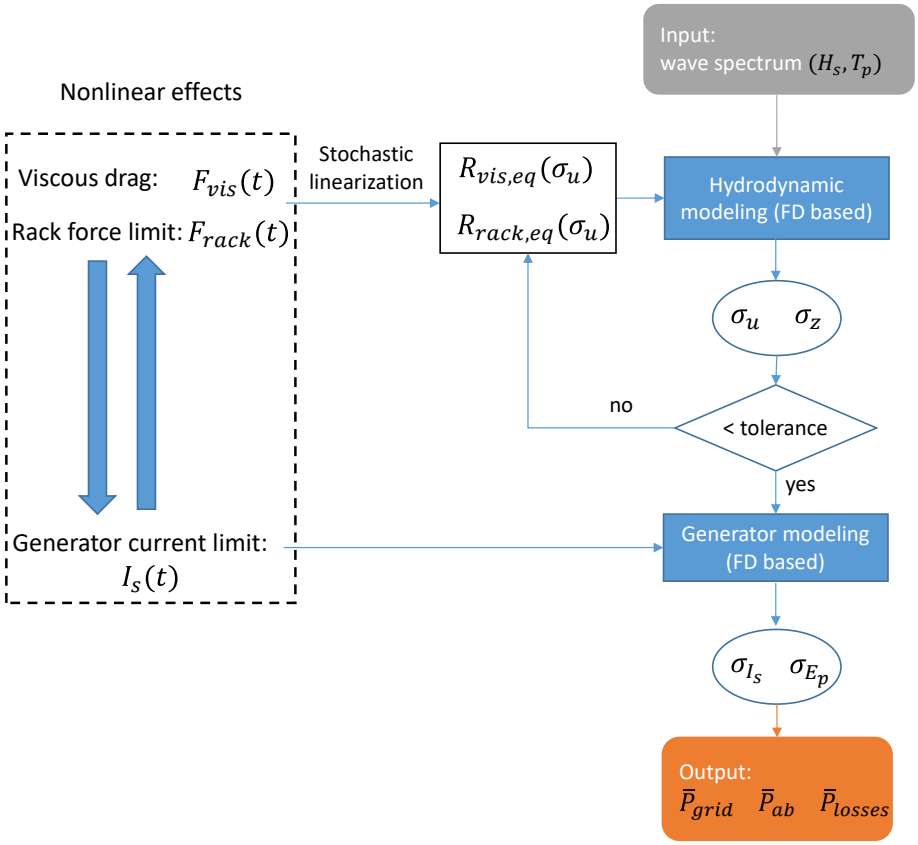

Fig. 2: Diagram of the proposed SD wave-to-wire modeling.

The power taken by the generator winding, namely P_{wd}, at each frequency component is calculated as

$$\begin{aligned} P_{wd}(\omega) &= \frac{1}{2}\mathrm{Re}\{\hat{F}_{rack}(\omega)\hat{u}^*(\omega)\} \\ &= \frac{1}{2}|\hat{F}_{rack}(\omega)||\hat{u}(\omega)| \\ &= \frac{1}{2}R_{rack,eq}|\hat{u}(\omega)|^2 \end{aligned} \tag{31}$$

Thus, the magnitude of the complex amplitude of the stator current at each frequency component can be calculated as

$$|\hat{I}_s(\omega)| = \frac{R_{rack,eq}|\hat{u}(\omega)|^2}{m|\hat{E}_p(\omega)|} \tag{32}$$

As the effect of the PTO force limit has been incorporated by the equivalent linear coefficient $R_{rack,eq}$, the current limit is therefore taking effect correspondingly. Then, the standard deviation of the stator current is derived as

$$\sigma_{I_s} = \sqrt{\frac{1}{2}\sum_{j=1}^{N}|I_s(\omega_j)|^2} \tag{33}$$

At this stage, the hydrodynamic, mechanical and electrical responses of the system can all be estimated using the SD modeling approach described earlier. However, to gain a deeper understanding of the generator's performance, it is necessary to determine the mechanical and electrical losses in the power transmission stages in the spectral domain context, consistent with the expressions used in the TD approach. Specifically, the gear friction losses in the rack and pinion system are calculated as

$$\begin{aligned} \overline{P}_{gear} &= < P_{gearm}\frac{|\omega_{ge}|}{\omega_{rated}} > \\ &= \frac{P_{gearm}}{\omega_{rated}} < |\omega_{ge}| > \end{aligned} \tag{34}$$

As ω_{ge} is assumed to be a Gaussian variable, the expected value of its absolute value is expressed as

$$< |\omega_{ge}| >= \sqrt{\frac{2}{\pi}}\sigma_{\omega_{ge}} \tag{35}$$

The copper losses of the generator can be calculated as follows:

$$\begin{aligned} \overline{P}_{copper} &= < mI_s^2 R_t > \\ &= mR_t\sigma_{I_s}^2 \end{aligned} \tag{36}$$

Assuming that the variable I_s follows the Gaussian distribution, it gives

$$< |I_s| >= \sqrt{\frac{2}{\pi}}\sigma_{I_s} \tag{37}$$

This enables the prediction of the converter losses, expressed as

$$\overline{P}_{conv} = \frac{1}{31}P_{convm} + \frac{20}{31I_{sm}}P_{convm} < |I_s| > + \frac{10}{31I_{sm}^2}P_{convm} < I_s^2 > \tag{38}$$

The iron losses are calculated as

$$\overline{P}_{Fes} = P_{Fe0}\left[m_{Fest}\left(\frac{\hat{B}_{st}}{B_0}\right)^2 + m_{Fesy}\left(\frac{\hat{B}_{sy}}{B_0}\right)^2\right]\frac{< f_e >}{f_0} \tag{39}$$

where $< f_e >$ can be related to the standard deviation of the absolute value of the buoy velocity, and assuming the Gaussian assumption of the response gives

$$\begin{aligned} < f_e > &=< \frac{2\pi}{2\tau_p}|\omega_{ge}|r_r > \\ &= \frac{2\pi}{2\tau_p} < |u| > R_{rp}r_r \\ &= \frac{\pi}{\tau_p}\sqrt{\frac{2}{\pi}}\sigma_u R_{rp}r_r \end{aligned} \tag{40}$$

Therefore, the mean grid power can be derived as

$$\overline{P}_{grid} = \overline{P}_{wd} - \overline{P}_{copper} - \overline{P}_{Fes} - \overline{P}_{gear} - \overline{P}_{conv} \tag{41}$$

3) Statistical linearization: The procedure for implementing statistical linearization of the relevant nonlinear effects in the hydrodynamic stage has been demonstrated in previous references [12], [13], [17]. Therefore, in this discussion, we will only provide a brief overview of the derivation of equivalent linear coefficients.

In the hydrodynamic stage, the equivalent linear coefficients $R_{\text{rack,eq}}$ and $R_{\text{vis,eq}}$ are considered to represent the effects of PTO force saturation and viscous force, respectively. The principle behind linearization is to achieve a balance between the expected value of the dissipated power and the power dissipated by an equivalent linear term. According to [12], the equivalent coefficient of a generic nonlinear force F_{non} in the hydrodynamic modeling can be calculated as follows:

$$\begin{aligned} R_{eq} &=< \frac{\partial F_{non}(u)}{\partial u} > \\ &= \int_{-\infty}^{\infty}\frac{\partial F_{non}(u)}{\partial u}p(u)\mathrm{d}u \end{aligned} \tag{42}$$

where F_{non} embodies the concerned nonlinear force, and $p(u)$ is the probability density function of the response u. Assuming the Gaussian process of the response, the probability density function is expressed as

$$p(u) = \frac{1}{\sigma_u\sqrt{2\pi}}\exp(-\frac{u^2}{2\sigma_u^2}) \tag{43}$$

With (43), the equivalent coefficients can be derived according to (42).

IV. Model Verification

This section presents the simulation results of the SD W2W model, validated against the TD model across various wave conditions. Figure 3 compares the standard deviation of the buoy velocity, the stator current, and the no-load voltage, along with the relative errors of the SD model. The maximum errors are 5% for the stator current, 6% for the no-load voltage, and 3% for the buoy velocity, increasing slightly with higher wave heights due to intensified nonlinear effects. The results present the demonstration of the effectiveness of the proposed model in estimating the dynamic and electrical responses of the WEC system.

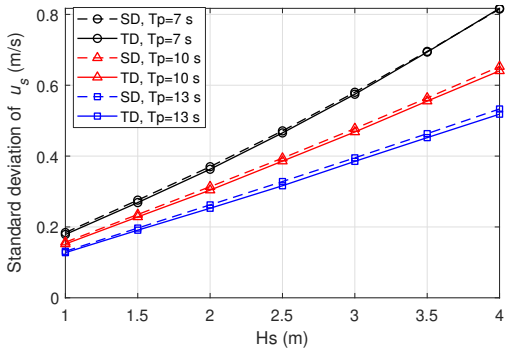

(a) Buoy velocity

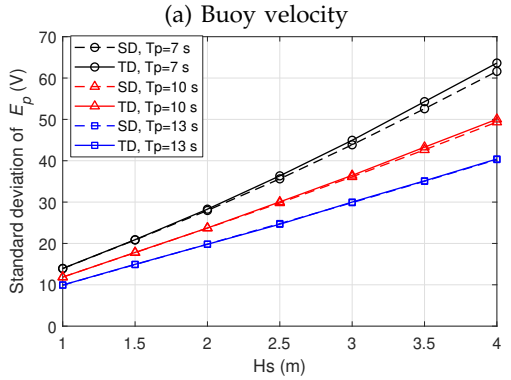

(b) No-load voltage

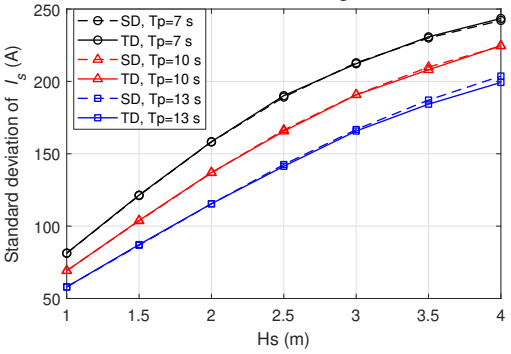

(c) Stator current

Fig. 3: The standard deviation of the responses of the WEC in different wave states of the SD W2W model to the TD W2W model. ($B_{pto} = 100$ kNs/m)

The W2W modeling framework enables a detailed assessment of power conversion efficiency across the entire system operation. To more comprehensively demonstrate the capability of the established SD W2W model, the losses at each power transmission stage, the electrical power supplied to the grid, and the corre-

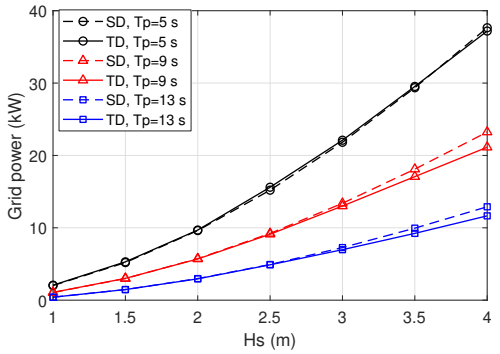

(a) Grid power

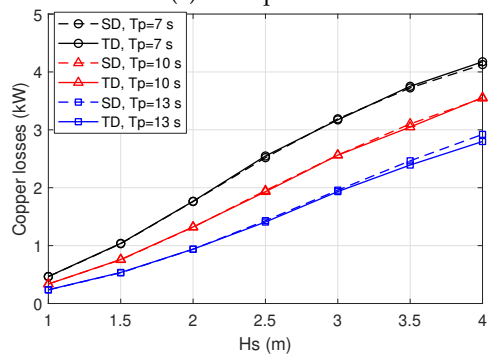

(b) Copper losses

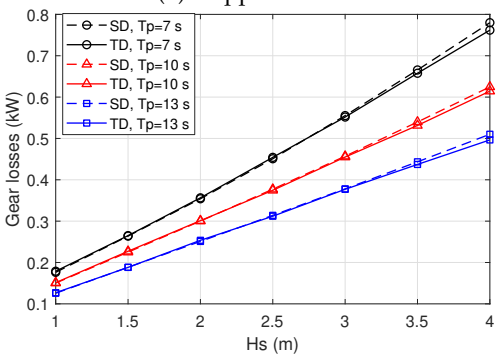

(c) Gear losses

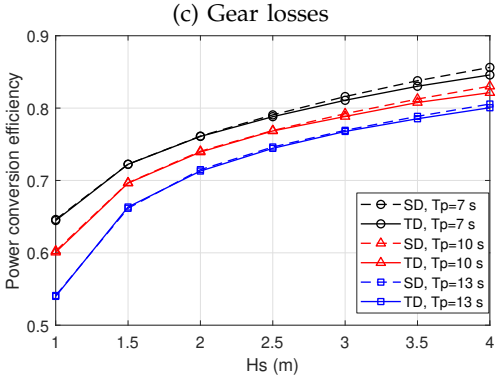

(d) Power conversion efficiency

Fig. 4: Grid power, copper losses and power conversion efficiency of the WEC in different wave states and the relative errors of the SD model to the TD model. ($B_{pto} = 60$ kNs/m)

sponding conversion efficiencies are evaluated against those evaluated by the TD model. Power conversion efficiency, measured as the ratio of electrical power delivered to the grid to the mechanical power absorbed by the floater, is a key performance metric in the performance assessment of WECs. Figure 4 presents the power, losses and the power conversion efficiencies estimated by the SD W2W and TD W2W models. Additionally, the relative errors of the proposed SD model to the TD W2W model are identified in Figure 5, in which their estimations of the grid power are taken into account. It is visible that the proposed SD model closely aligns with the TD model in estimating the results in different operation stages, maintaining relative errors below 6% even at a significant wave height of 4 m and under 2% for milder sea states ($H_s < 2.5$ m). These observations imply that the SD model's reliability in estimating power conversion efficiency. As a consequence, the proposed SD W2W model can be applied as an effective alternative to the TD W2W models to analyze the systematic performance or perform design optimizations of WECs.

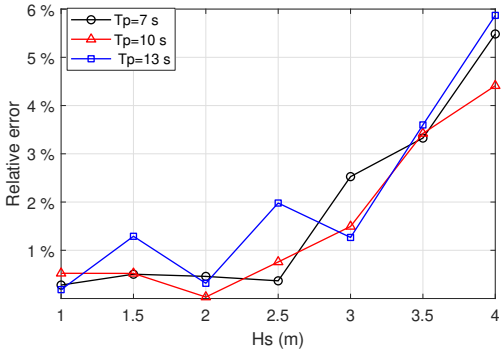

Fig. 5: The relative errors of the established SD W2W model to the TD W2W model with regard to the grid power estimation.

V. Computational Efficiency

Simulating the whole W2W process in the conventional TD modeling approach is particularly time-demanding. Comparatively, the most featuring merit of the SD modeling is high computational efficiency compared to its reference TD modeling. Figure 6 shows the computational time of the proposed SD W2W model normalized to that of the applied TD W2W model. It is noted that the normalized computational time decreases with lowering the iteration tolerance in the SD W2W model. The reason is that lower tolerance requires a larger number of numerical iterations. Nevertheless, the SD W2W model is over thousand times faster than the TD W2W model while the tolerance is defined as strict as $1e^{-3}$

VI. Conclusion

A spectral-domain (SD) wave-to-wire (W2W) model is developed for a spherical point absorber using a rotary PM generator coupled with a rack and pinion system. Statistical linearization accounts for nonlinear effects in both hydrodynamic and electrical stages. The proposed SD W2W model can be used to estimate the statistical forms of responses, losses and power in different power transmission stages.

The proposed SD W2W model offers not only high computational efficiency but also adequate accuracy.

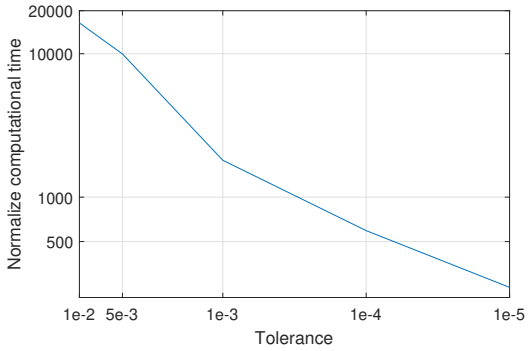

Fig. 6: The computational time of the SD W2W model to that of the TD W2W model. The simulation case was run with inputs of $Hs = 3m$ and $Tp = 7s$.

Given a reasonable iteration tolerance of $1e^{-3}$ implemented in the SD W2W model, it outperforms the corresponding TD W2W model by over 1000 times in speed. In addition, the SD W2W model is validated against a nonlinear TD W2W model, demonstrating high accuracy and computational efficiency, with relative errors below 6 % under typical WEC operating conditions.

Given the verified accuracy, the proposed SD W2W method can be generalized in the future to tackle other types of PTO mechanisms or multi-degrees-of-freedom WECs. In addition, the proposed model is only verified against a higher-fidelity TD model in the current work. An experimental validation could better confirm the performance of the SD model.

REFERENCES

[1] M. Penalba and J. V. Ringwood, "A review of wave-to-wire models for wave energy converters," *Energies*, vol. 9, no. 7, 2016.
[2] M. Folley, *Numerical Modelling of Wave Energy Converters*, 2016.
[3] M. Penalba and J. V. Ringwood, "A high-fidelity wave-to-wire model for wave energy converters," *Renewable energy*, vol. 134, pp. 367–378, 2019.
[4] M. Penalba, N. P. Sell, A. J. Hillis, and J. V. Ringwood, "Validating a wave-to-wire model for a wave energy converter—part i: The hydraulic transmission system," *Energies*, vol. 10, no. 7, p. 977, 2017.
[5] M. Penalba, J.-A. Cortajarena, and J. V. Ringwood, "Validating a wave-to-wire model for a wave energy converter—part ii: The electrical system," *Energies*, vol. 10, no. 7, p. 1002, 2017.
[6] J. Hals, J. Falnes, and T. Moan, "Constrained Optimal Control of a Heaving Buoy Wave-Energy Converter," *Journal of Offshore Mechanics and Arctic Engineering*, vol. 133, no. 1, p. 011401, 2010.
[7] J. Tan, H. Polinder, P. Wellens, and S. Miedema, "A feasibility study on downsizing of power take off system of wave energy converters," in *Developments in Renewable Energies Offshore*. CRC Press, 2020, pp. 140–148.
[8] D. Son and R. W. Yeung, "Real-time implementation and validation of optimal damping control for a permanent-magnet linear generator in wave energy extraction," *Applied Energy*, vol. 208, pp. 571–579, 2017.
[9] R. G. Coe and G. Bacelli, "Useful power maximization for wave energy converters," p. 529, 2023.
[10] J. Tan, X. Wang, H. Polinder, A. J. Laguna, and S. A. Miedema, "Downsizing the linear pm generator in wave energy conversion for improved economic feasibility," *Journal of Marine Science and Engineering*, vol. 10, no. 9, p. 1316, 2022.
[11] J. Tan, X. Wang, A. Jarquin Laguna, H. Polinder, and S. Miedema, "The influence of linear permanent magnet generator sizing on the techno-economic performance of a wave energy converter," in *2021 13th International Symposium on Linear Drives for Industry Applications (LDIA)*, 2021, pp. 1–6.
[12] M. Folley and T. Whittaker, "Spectral modelling of wave energy converters," *Coastal Engineering*, vol. 57, no. 10, pp. 892–897, 2010.
[13] J. Tan, H. Polinder, A. J. Laguna, and S. Miedema, "The application of the spectral domain modeling to the power take-off sizing of heaving wave energy converters," *Applied Ocean Research*, vol. 122, p. 103110, 2022.
[14] A. De O Falcão and R. Rodrigues, "Stochastic modelling of owc wave power plant performance," *Applied Ocean Research*, vol. 24, no. 2, pp. 59–71, 2002.
[15] L. S. P. d. Silva, "Nonlinear stochastic analysis of wave energy converters via statistical linearization." Ph.D. dissertation, Universidade de São Paulo, 2019.
[16] L. S. da Silva, B. S. Cazzolato, N. Y. Sergiienko, B. Ding, H. M. Morishita, and C. P. Pesce, "Statistical linearization of the morison's equation applied to wave energy converters," *Journal of Ocean Engineering and Marine Energy*, vol. 6, no. 2, pp. 157–169, 2020.
[17] L. Silva, N. Sergiienko, C. Pesce, B. Ding, B. Cazzolato, and H. Morishita, "Stochastic analysis of nonlinear wave energy converters via statistical linearization," *Applied Ocean Research*, vol. 95, p. 102023, 2020.
[18] P. D. Spanos, F. M. Strati, G. Malara, and F. Arena, "An approach for non-linear stochastic analysis of u-shaped owc wave energy converters," *Probabilistic Engineering Mechanics*, vol. 54, pp. 44–52, 2018.
[19] S. Gunawardane, M. Folley, and S. Sanjaya, "Spectral-domain modelling of the non-linear hydrostatic stiffness of a heaving-sphere wave energy converter," in *Proceedings of the 28th International Symposium on Transport Phenomena, Peradeniya, Sri Lanka*, 2017, pp. 22–24.
[20] J. Tan, W. Tao, A. J. Laguna, H. Polinder, Y. Xing, and S. Miedema, "A spectral-domain wave-to-wire model of wave energy converters," *Applied Ocean Research*, vol. 138, p. 103650, 2023.
[21] J. Tan and A. J. Laguna, "Spectral-domain modelling of wave energy converters as an efficient tool for adjustment of pto model parameters," in *Proceedings of the European Wave and Tidal Energy Conference*, vol. 15, 2023.
[22] H. Polinder, M. E. C. Damen, and F. Gardner, "Linear PM generator system for wave energy conversion in the AWS," *IEEE Transactions on Energy Conversion*, vol. 19, no. 3, pp. 583–589, 2004.
[23] H. Polinder, F. F. Van der Pijl, G.-J. De Vilder, and P. J. Tavner, "Comparison of direct-drive and geared generator concepts for wind turbines," *IEEE Transactions on energy conversion*, vol. 21, no. 3, pp. 725–733, 2006.
[24] Johannes Falnes, *Ocean waves and Oscillating systems*, 2003.
[25] J. M. J. Journée, W. W. Massie, and R. H. M. Huijsmans, *Offshore hydrodynamics*, 2015.
[26] W. Cummins, W. Iiuhl, and A. Uinm, "The impulse response function and ship motions," 1962.
[27] M. Penalba, T. Kelly, and J. Ringwood, "Using NEMOH for Modelling Wave Energy Converters : A Comparative Study with WAMIT," *12th European Wave and Tidal Energy Conference*, p. 10, 2017.
[28] T. Pérez and T. Fossen, "Time-vs. frequency-domain identification of parametric radiation force models for marine structures at zero speed," *Modeling, Identification and Control*, vol. 29, no. 1, pp. 1–19, 2008.
[29] G. Giorgi and J. V. Ringwood, "Consistency of viscous drag identification tests for wave energy applications," *12th European Wave and Tidal Energy Conference*, pp. 1–8, 2017.
[30] H. Polinder, F. van der Pijl, G.-J. de Vilder, and P. Tavner, "Comparison of direct-drive and geared generator concepts for wind turbines," *IEEE Transactions on Energy Conversion*, vol. 21, no. 3, pp. 725–733, 2006.
[31] M. Folley and T. Whittaker, "Validating a spectral-domain model of an owc using physical model data," *International Journal of Marine Energy*, vol. 2, pp. 1–11, 2013.
[32] A. Pecher, *Handbook of Ocean Wave Energy*, 2017, vol. 7. [Online]. Available: http://link.springer.com/10.1007/978-3-319-39889-1